Human Molecular Genetics, 2011, Vol. 20, No. 10 **2015–2025**
doi:10.1093/hmg/ddr084
Advance Access published on February 28, 2011

Changes in cross-bridge cycling underlie muscle weakness in patients with tropomyosin 3-based myopathy

Coen A.C. Ottenheijm[1,2,*], Michael W. Lawlor[3], Ger J.M. Stienen[1], Henk Granzier[2] and Alan H. Beggs[3,*]

[1]Department of Physiology, Institute for Cardiovascular Research, VU University Medical Center, Amsterdam 1081 BT, The Netherlands, [2]Department of Physiology, University of Arizona, Tucson, AZ 85724, USA and [3]Division of Genetics and Program in Genomics, The Manton Center for Orphan Disease Research, Children's Hospital Boston, Harvard Medical School, Boston, MA 02115, USA

Received November 30, 2010; Revised February 4, 2011; Accepted February 22, 2011

Nemaline myopathy, the most common non-dystrophic congenital myopathy, is caused by mutations in six genes, all of which encode thin-filament proteins, including *NEB* (nebulin) and *TPM3* (α tropomyosin). In contrast to the mechanisms underlying weakness in *NEB*-based myopathy, which are related to loss of thin-filament functions normally exerted by nebulin, the pathogenesis of muscle weakness in patients with *TPM3* mutations remains largely unknown. Here, we tested the hypothesis that the contractile phenotype of *TPM3*-based myopathy is different from that of *NEB*-based myopathy and that this phenotype is a direct consequence of the loss of the specific functions normally exerted by tropomyosin. To test this hypothesis, we used a multidisciplinary approach, including muscle fiber mechanics and confocal and electron microscopy to characterize the structural and functional phenotype of muscle fibers from five patients with *TPM3*-based myopathy and compared this with that of unaffected control subjects. Our findings demonstrate that patients with *TPM3*-based myopathy display a contractile phenotype that is very distinct from that of patients with *NEB*-based myopathy. Whereas both show severe myofilament-based muscle weakness, the contractile dysfunction in *TPM3*-based myopathy is largely explained by changes in cross-bridge cycling kinetics, but not by the dysregulation of sarcomeric thin-filament length that plays a prominent role in *NEB*-based myopathy. Interestingly, the loss of force-generating capacity in *TPM3*-based myopathy appears to be compensated by enhanced thin-filament activation. These findings provide a scientific basis for differential therapeutics aimed at restoring contractile performance in patients with *TPM3*-based versus *NEB*-based myopathy.

INTRODUCTION

The skeletal muscle sarcomere consists of thick filaments, mainly comprised of myosin, and the actin-based thin filaments. In addition to actin, major components of the thin filament include tropomyosin (Tm), the troponin complex and nebulin (1). The thin filament plays several key roles in the regulation of muscle contraction. First, the length of the thin filament determines the amount of overlap between the thick and the thin filaments, which, in turn, determines the number of myosin–actin interactions (i.e. cross-bridges) and thus the sarcomere's force-generating capacity (2). Recent studies suggest that thin-filament length is regulated by nebulin, a giant protein that spans the entire length of the thin filament and that the absence of nebulin causes shortening and non-uniformity of thin-filament length (3–6). Second, the

*To whom correspondence should be addressed at: VU University Medical Center, Department of Physiology, Institute for Cardiovascular Research, 1081 BT Amsterdam, The Netherlands. Tel: +31 204448123; Fax: +31 204448255; Email: c.ottenheijm@vumc.nl (C.O.); Division of Genetics and Program in Genomics, The Manton Center for Orphan Disease Research, Children's Hospital Boston, Harvard Medical School, 300 Longwood Ave., Boston, MA 02115, USA. Tel: +1 6179192170; Fax: +1 6177300786; Email: beggs@enders.tch.harvard.edu (A.H.B.)

regulatory proteins Tm and troponin control thin-filament activation by a mechanism in which Ca^{2+} binding to troponin moves Tm over the surface of actin to expose myosin binding sites on actin. Myosin then binds on actin to form cross-bridges and propel muscle contraction. The key role of the thin filament in the regulation of muscle contraction has been emphasized by the identification of mutations within genes encoding thin filament proteins in patients with congenital myopathies (7).

Nemaline myopathy (NM), the most common non-dystrophic congenital myopathy, is caused by mutations in six genes, all of which encode thin filament proteins: *ACTA1* (actin), *TPM3* and *TPM2* (α- and β-Tm, respectively), *TNNT1* (troponin T), *CFL2* (cofilin-2) (8) and *NEB* (nebulin), for a review see Sanoudou and Beggs (9). Hence, NM is often considered a thin filament myopathy. The main form of NM, likely accounting for ∼50% of all NM cases, results from mutations in *NEB* (10), which encodes nebulin, a giant protein (MW ∼800 kDa) that is expressed at high levels only in skeletal muscle. Recent studies on muscle fibers from patients suffering from NM due to *NEB* mutations revealed that the muscle fiber weakness observed in these patients can be largely explained by changes in thin filament length (6), cross-bridge cycling kinetics and Ca^{2+} sensitivity (11). This phenotype shows remarkable similarities to that of myofibers from nebulin KO mice (3,6,12,13), suggesting that nebulin abnormalities and nebulin absence both cause weakness through similar pathogenic mechanisms.

Mutations in the Tm 3 gene (*TPM3*), which encodes for $\alpha\text{-Tm}_{slow}$, can cause both NM, as well as congenital fiber-type disproportion (CFTD) (14–19). Similar to the patients with *NEB* mutations, the hallmark feature of these patients is skeletal muscle weakness. However, in contrast to the mechanisms underlying weakness in *NEB*-based myopathy that are related to loss of thin filament functions normally exerted by nebulin (6,11), the pathogenesis of muscle weakness in patients with *TPM3* mutations remains largely unknown.

A common histopathological finding in many cases with *TPM3* mutations is selective type 1 fiber hypotrophy/atrophy (19), presumably because *TPM3* is primarily expressed in type 1 fibers. However, this phenotype can only partly explain the muscle weakness observed in these patients. Considering that Tm plays distinct roles in thin filament function, we expect that loss of these functions due to genetic mutations might very well contribute to thin filament dysfunction and muscle weakness in patients. Thus, we hypothesize that the contractile phenotype of *TPM3*-based myopathy is different from that of *NEB*-based myopathy and that this phenotype is a direct consequence of the loss of the specific functions normally exerted by Tm. To test this hypothesis, we used a multidisciplinary approach to characterize the structural and functional phenotype of muscle fibers from patients with *TPM3*-based myopathy.

RESULTS

Tm protein levels in patients with *TPM3*-based myopathy

To characterize the effects of the gene mutations on protein expression, western blot analysis was performed for Tm in muscle biopsies from five patients with *TPM3*-based myopathy and four control subjects. Similar to control subjects, muscle from all five patients showed expression of both α- and β-Tm (Fig. 1A, bottom panel). However, patients T7 and T261, which had the autosomal recessive mutation c.857A > C (p.X286SerextX*57), showed an additional, novel band ∼6 kDa larger, representing the additional 57 amino acids following the read-through Stop → Ser change (16,19). Importantly, the mutations in *TPM3* do not appear to affect the ratio of α-Tm over β-Tm (Fig. 1A, top left). Also, total Tm normalized to actin was comparable between patients and controls (Fig. 1A, top right). In summary, the levels of Tm isoform expression in skeletal muscle of these five patients with *TPM3*-based myopathy are comparable with that found in controls.

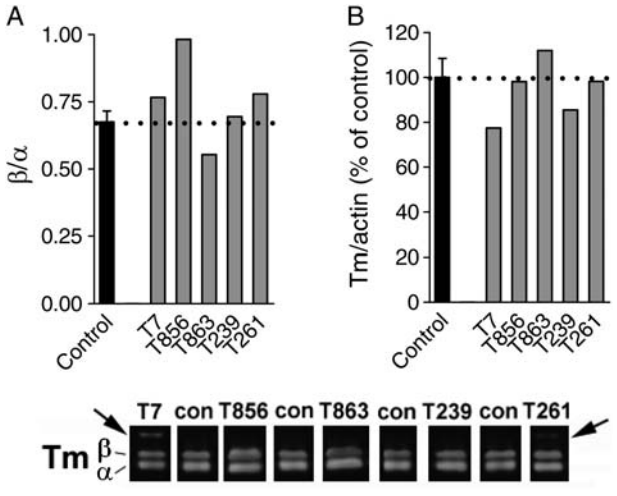

Figure 1. (**A**) The ratio of β-Tm over α-Tm was comparable between the muscle specimens from controls and those from patients with *TPM3*-based myopathy. (**B**) Total Tm, normalized to actin, was comparable between controls and patients. Bottom: typical Tm western blot result; note the additional band with higher molecular weight in two patients (T7 and T261) who carry the c.857A > C mutation that eliminates the stop codon.

Severe muscle fiber weakness in patients with *TPM3*-based myopathy

To study whether the muscle weakness observed in patients with *TPM3* mutations is caused by changes in myofilament function, we studied the force-generating capacity of small muscle fiber bundles from patients with *TPM3*-based myopathy and of single muscle fibers from control subjects. We exposed skinned muscle fibers to a saturating Ca^{2+} concentration and measured the force response; Figure 2A shows a typical force response from a control and patient muscle fiber. As force is proportional to the muscle fiber's cross-sectional area (CSA), force was normalized to fiber CSA to obtain stress. We found that maximal stress generation was severely reduced in muscle fibers from all five patients with *TPM3* mutations (Fig. 2B). Because Ca^{2+} handling proteins are absent in skinned fibers, these findings suggest severely impaired myofilament function in skeletal muscle from patients with *TPM3*-based myopathy. Considering that the contractile experiments on patient biopsies were performed using preparations containing multiple (10–20) muscle fibers

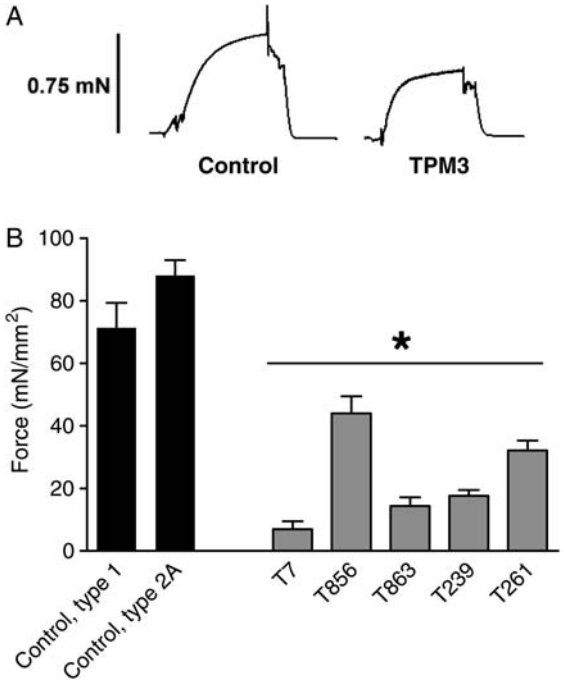

Figure 2. (**A**) Typical force response to saturating Ca^{2+} levels of a control fiber and a fiber from a patient with *TPM3*-based myopathy (T856 is shown) with similar fiber CSAs. Note the lower maximal force in the fiber from the patient. (**B**) The maximal force-generating capacity was significantly decreased in muscle fiber bundles from patients with *TPM3*-based myopathy. Values shown are the mean ± SEM. $^{*}P < 0.05$ compared with both type 1 and 2A fibers from controls.

and that type 1 fibers were hypotrophic, the majority of the preparations' volume was comprised of type 2A fibers. Thus, these findings suggest that the functioning of type 2A fibers is also affected in patients with *TPM3*-based myopathy.

Preserved thin filament length in myofibrils from patients with *TPM3*-based myopathy

Previous work on NM patients with mutations in the gene encoding nebulin, another major constituent of the sarcomere thin filament, revealed that the muscle weakness in those patients was at least partly caused by a reduced length of the thin filaments of the sarcomere (6). To study whether the muscle fiber weakness in patients with *TPM3*-based myopathy can be explained by similar changes in thin filament length, we investigated thin filament length using immunofluorescence confocal scanning laser microscopy on small muscle fiber bundles. We first localized α-actinin, a Z-disk marker and tropomodulin, a thin filament pointed-end capping protein that has been used previously by us and by others as a determinant of thin filament length (5,6,20). α-Actinin staining showed regular striation patterns in myofibrils from both controls and patients (Fig. 3A), indicating well-organized myofibrillar structure. In control myofibrils, tropomodulin staining showed a distinct doublet in the middle of the sarcomere, 2.66 ± 0.08 μm apart (measured across the Z-disk, Fig. 3A). Similarly, in myofibrils from patients, tropomodulin staining revealed a doublet in the middle of the sarcomere, 2.50 ± 0.09 μm apart. This difference between control subjects and *TPM3*-based myopathy patients was not significantly different, suggesting that thin filament lengths are comparable between patients with *TPM3*-based myopathy and controls, with an average length of 1.25–1.30 μm. Note that for these measurements, muscle fiber bundles were studied, which consist of both type 1 and 2A muscle fibers, and these thin filament lengths reflect those found in both fiber types.

Confocal microscopy studies with fluorescently labeled phalloidin (which binds filamentous actin with high affinity) were also carried out. The labeling patterns of myofibrils from patients and controls were similar: both patients and controls showed broad actin labeling with uniform intensity, except for the Z-disk area where actin filaments overlap to produce stronger intensity (Fig. 3B, left panel). Densitometric analysis revealed that the width at half-maximal intensity was 2.40 ± 0.04 μm for controls and 2.40 ± 0.09 μm for myofibrils from patients (Fig. 3B, right panel). Thus, in line with the tropomodulin data, phalloidin staining studies indicate that thin filament lengths are comparable between myofibrils from controls and those from patients with *TPM3*-based myopathy.

Because sarcomeres generate force in proportion to the degree of thick and thin filament overlap, a well-defined thin filament length is an important determinant of proper muscle function. This is illustrated by the force–sarcomere length (SL) relation, which is characterized by a force plateau at optimal filament overlap, followed by a descending limb at higher SLs as filament overlap decreases. Since thick filaments are typically of a constant length and thin filament lengths are comparable between patients and controls (Fig. 3A and B), the force–SL relations of myofibrils from patients and controls are expected to overlap. To test this expectation, we constructed force–SL relations of control and patient muscle by activating skinned muscle fiber bundles at various SLs (Fig. 3C, top panel, shows a typical force response at a range of SLs). Control fibers showed a characteristic force plateau up to ∼2.8 μm, followed by a linear descending limb (Fig. 3C). Thus, these functional data from control myofibrils are in line with thin filaments of a uniform and well-defined length. As expected from our confocal imaging data, fibers from patients exhibit a force–SL relation that is comparable with control fibers. Thus, these structural and functional data suggest that changes in thin filament length cannot explain the muscle fiber weakness in patients with *TPM3*-based myopathy.

Preserved myofibrillar structure in muscle from patients with *TPM3*-based myopathy

To test whether the observed muscle fiber weakness is caused by disorganization or disruption of myofibrillar structure, we performed light- and electron-microscopic analyses. As shown in Figure 4, and as reported previously (19), patients with *TPM3*-based myopathy invariably showed a selective type 1 fiber hypotrophy (Fig. 4Aa and b), and the proportions of type 1 and 2 fibers are often within normal limits or show type 1 fiber predominance. Longitudinal sections of toluidine blue stained tissue revealed a regular distribution of sarcomeres

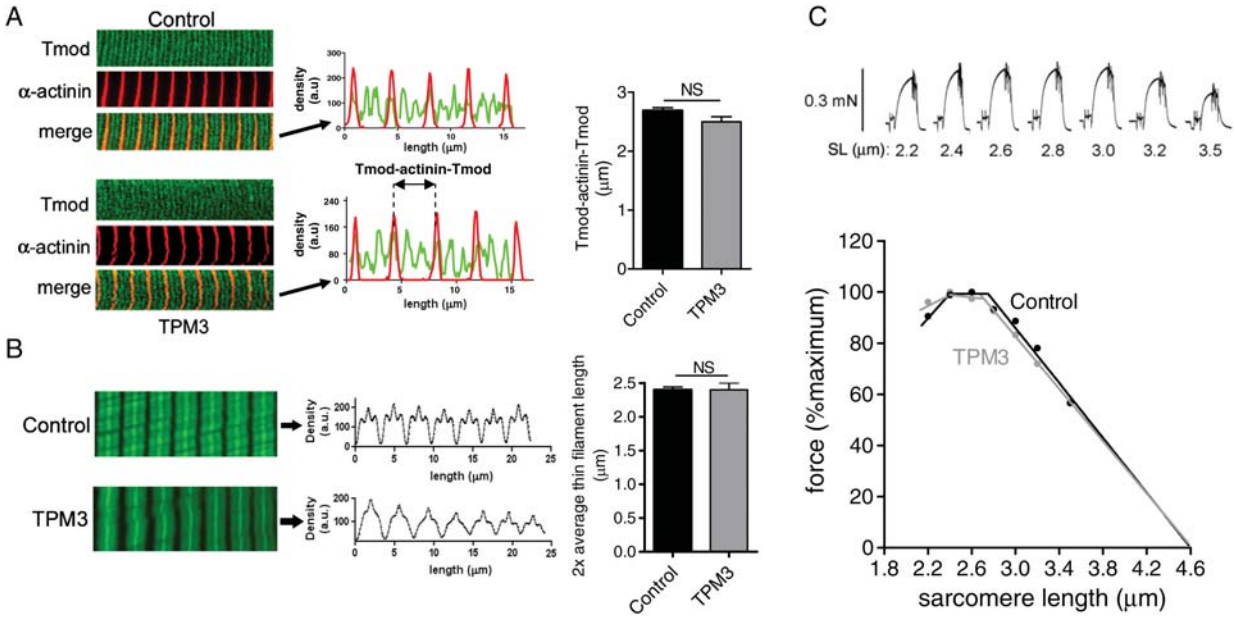

Figure 3. (**A**) Representative images and analysis of myofibrils from controls and patients with *TPM3*-based myopathy stained for α-actinin and tropomodulin (Tmod). Left: note the tropomodulin doublet in the middle of the sarcomere in the control and in the patients' myofibrils (biopsy T239 is shown). Middle: overlay of line scan intensity profile of α-actinin and tropomodulin. Right: the distance between tropomodulin staining (measured across the Z-disk and indicated as Tmod-α-actinin-Tmod) is comparable between control and patient myofibrils. (**B**) Left: actin staining with phalloidin shows broad and homogenous staining in both control myofibrils and myofibrils from patients with *TPM3*-based myopathy (note that the fainter phalloidin staining of myofibrils from the TPM3 patient depicted here was not a consistent finding). Middle and right: analysis of phalloidin line scan intensities revealed comparable average thin filament lengths in control and patient myofibrils. (**C**) Top: typical force response of a patient's muscle fiber preparation that was activated at various SLs. Bottom: the force–SL relation of fiber preparations from patients with *TPM3*-based myopathy overlap with that from control fibers: both display a characteristic force plateau followed by a comparable descending limb. NS, not significant. Values shown are the mean ± SEM.

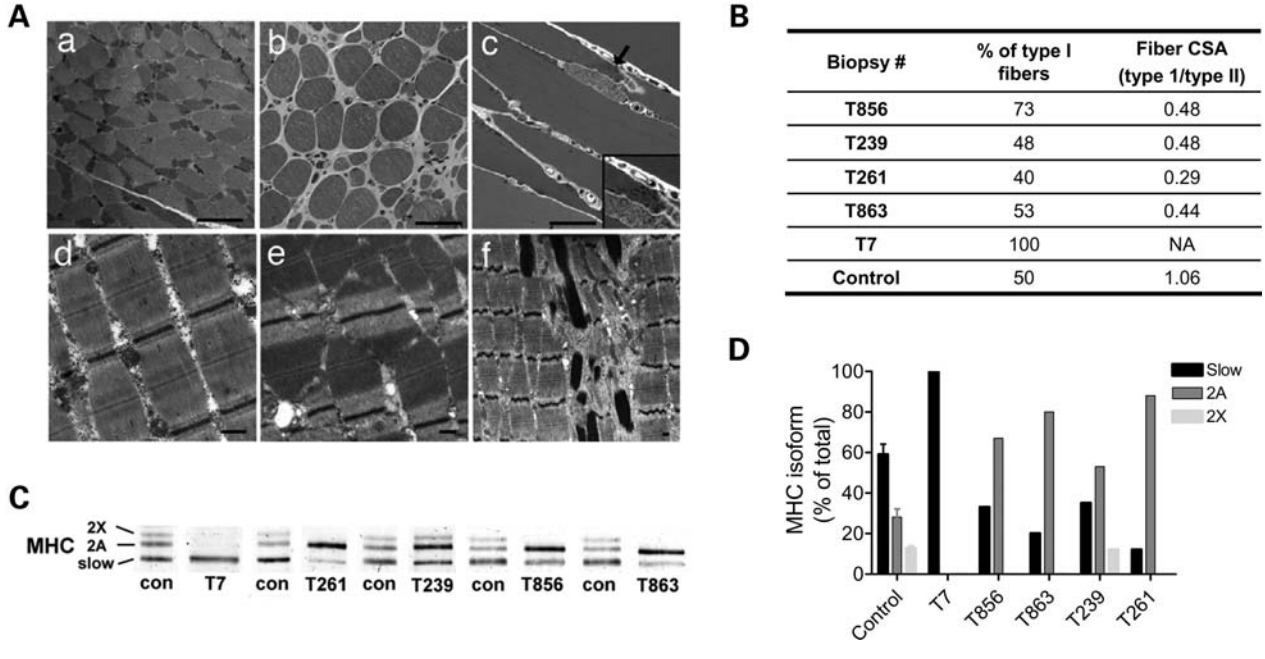

Biopsy #	% of type I fibers	Fiber CSA (type 1/type II)
T856	73	0.48
T239	48	0.48
T261	40	0.29
T863	53	0.44
T7	100	NA
Control	50	1.06

Figure 4. (**A**) Muscle histology and ultrastructure in patients with *TPM3* mutations. Toluidine blue staining (a–c) of Epon-embedded tissue from biopsy (a and d) T863, (b and e) T261 and (c and f) T856 reveals increased variation in fiber size, which corresponds to the selective hypotrophy of type 1 fibers on oxidative stains (a). A subsarcolemmal aggregate of nemaline rods is seen in one fiber from biopsy T856 (c). Ultrastructural examination of muscle from these patients reveals an appropriate organization of the contractile apparatus (d and e), with the exception of areas containing nemaline rods in biopsy T856 (f). Note that the "out of register" appearance of the sarcomeres in (e) is a normal finding that is often due to inadequate stretching of the muscle during fixation or the oblique orientation of the section. Bar = 50 μm for a–c and 500 nm for d–f. (**B**) Table showing the fiber-type proportions and the relative fiber CSAs for controls and patients. Note the variable degrees of type 1 predominance, but consistent type 1 fiber hypotrophy in patients. (**C**) Typical SDS–PAGE result showing the relative contributions of the various myosin heavy chain (MHC) isoforms in the different biopsies (indicated below). (**D**) In line with the histology data, quantification of the myosin heavy chain isoforms obtained from the SDS–PAGE results revealed a decreased proportion of type 1 isoforms in muscle biopsies from patients (with the exception of T7), reflecting the type 1 fiber hypotrophy.

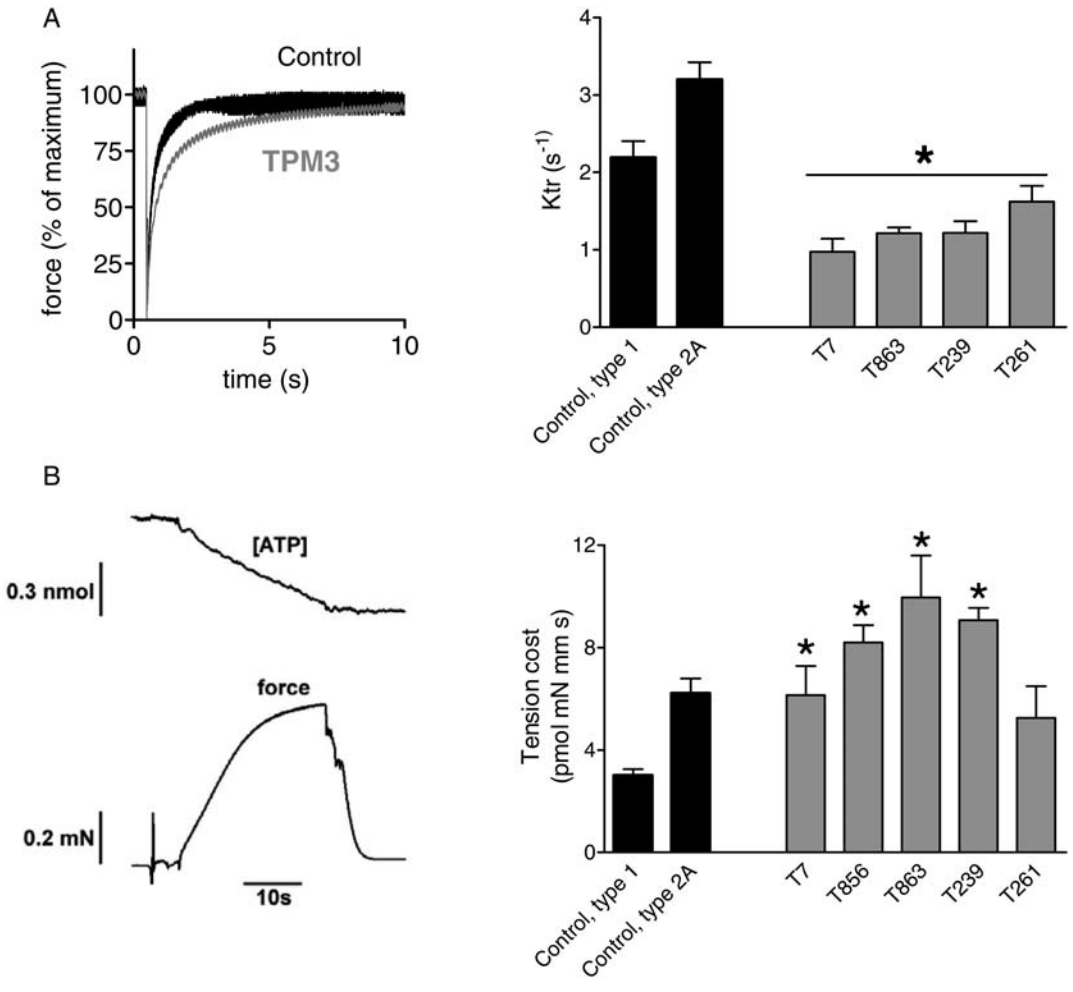

Figure 5. (**A**) k_{tr} measurements of fibers from controls and patients with *TPM3*-based myopathy. Left: example of typical k_{tr} measurements at pCa 4.5 with superimposed results of a patient fiber bundle (biopsy T239 is shown) and a control fiber. Right: k_{tr} is significantly lower in fibers from patients compared with control fibers. (**B**) Tension cost of patient and control myofibers. Left: example of a maximally activated patient fiber bundle (pCa 4.5) with developed force at the bottom and [ATP] at the top. The slope of the [ATP] versus time trace was divided by fiber volume (in mm^3) to determine the ATP consumption rate. Right: the ATP consumption rate was normalized to tension to determine the tension cost. The tension cost is significantly higher in fibers from patients with *TPM3*-based myopathy. Values shown are the mean ± SEM. $^*P < 0.05$ compared with both type 1 and 2A fibers from controls.

throughout muscle fibers of both types, with the exception of small areas that were occupied by nemaline rods in the two biopsies from patients with NM (Fig. 4Ac). As previously reported, nemaline rods, where present, were restricted to type 1 fibers and occupied a very small percentage (estimated at <5%) of the fiber CSA on longitudinal sections (19,21). Consistent with these findings, analysis of myosin heavy chain expression revealed that, with the exception of T7, which expressed solely myosin heavy chain type 1, patients had an elevated proportion of type 2 myosin heavy chain when compared with controls (Fig. 4C and D), which is likely to be a reflection of the type 1 fiber hypotrophy.

Ultrastructural examination revealed an appropriate organization of the contractile apparatus in patients with *TPM3*-based myopathy (Fig. 4Ad and e), with the exception of areas containing nemaline rods in the two patients with NM (for an example, see Fig. 4A f). Thus, these analyses indicate preserved myofibrillar structure in patients with *TPM3*-based myopathy.

Altered cross-bridge cycling kinetics in patients with *TPM3*-based myopathy

It is well established that Tm plays an important role in muscle function by regulating the cyclic interaction between myosin heads and actin (i.e. cross-bridge cycling kinetics) through limiting access to myosin head binding sites on the actin filament (1). To study whether changes in cross-bridge cycling kinetics play a role in the muscle fiber weakness in patients with *TPM3*-based myopathy, we determined the rate of tension redevelopment (k_{tr}) and the tension cost in muscle fiber bundles. To determine k_{tr}, muscle fiber preparations were first isometrically activated at pCa 4.5, and when a steady tension was reached, cross-bridges were disengaged by performing a quick release, a brief period of unloaded shortening and then a rapid restretch to the original length. Following restretch, tension rebuilds with a time course that can be fit to a monoexponential with rate constant k_{tr}. Figure 5A (left panel) illustrates a k_{tr} measurement on a

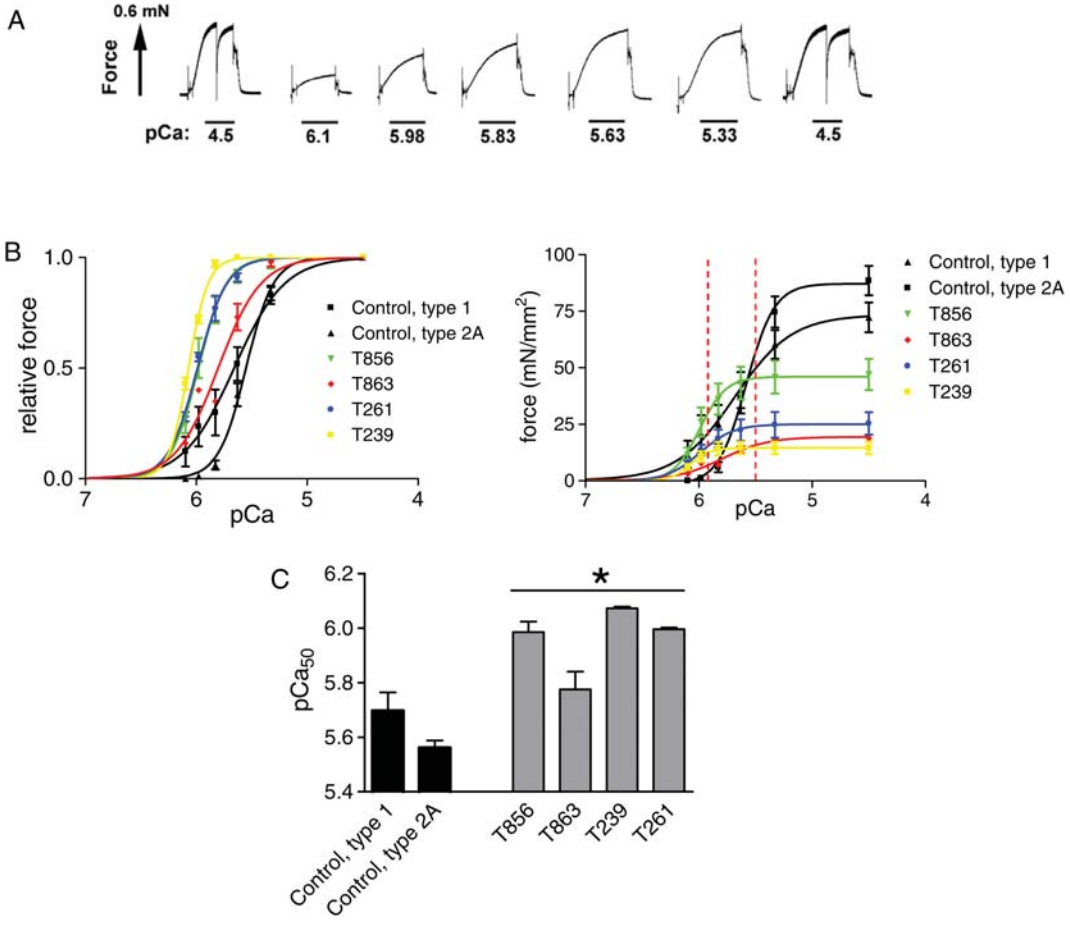

Figure 6. Force–Ca^{2+} characteristics of skinned muscle from patients with *TPM3*-based myopathy and from control muscle. (**A**) Typical chart recording showing the force response to incremental Ca^{2+} concentrations in a patient's fiber preparation (biopsy T856 is shown). (**B**) Left: the relative force generated in response to incubation with incremental increase of [Ca^{2+}]; note the leftward shift of the force–Ca^{2+} relationship in patients' versus control muscle fibers. Right: same as left panel, but with force normalized to the fiber CSA. The red dotted lines indicate *in vivo* cytosolic Ca^{2+} concentrations during activation. Note that T856 produces higher force at these Ca^{2+} levels than control fibers. (**C**) The Ca^{2+} concentration needed for 50% of maximal force generation was significantly lower (i.e. higher pCa_{50}) in patient versus control muscle. Values shown are the mean ± SEM. $^{*}P < 0.05$ compared with both type 1 and 2A fibers from controls.

patient and control fiber preparation, revealing that tension recovers more slowly in the patient fibers than in the control fibers. The averaged results from all subjects are shown in Figure 5A (right panel). k_{tr} is significantly lower in fibers from all patients with *TPM3*-based myopathy compared with control fibers.

The tension cost was determined by the measurement of the breakdown of nicotinamide adenine dinucleotide (NADH) simultaneous with force during contraction with NADH levels enzymatically coupled to adenosine triphosphate (ATP) utilization (see Materials and methods). An example of a maximally activated patient's muscle fiber preparation with [NADH] falling linearly during the tension plateau is shown in Figure 5B (left panel). The slope of the [NADH] versus time curve was normalized by the fiber volume to obtain ATP consumption rates that can be compared for differently sized muscle preparations. By normalizing the ATP consumption rates to the tension generated and fiber volume, the tension cost can be determined. As shown in Figure 5B (right panel), the tension cost was significantly higher in muscle fiber preparations from patients compared with those from control fibers, with the exception of biopsy T261 in which the fibers showed slightly elevated tension costs that were not statistically different from controls. Note that as T7 solely expressed type 1 myosin heavy chains, the tension cost data from this patient were compared with the data from type 1 fibers from controls. Thus, these k_{tr} and tension cost data suggest that cross-bridge cycling kinetics are significantly altered in muscle fibers from patients with *TPM3*-based myopathy.

Elevated Ca^{2+} sensitivity of force generation in patients with *TPM3*-based myopathy

In vivo, skeletal muscle typically undergoes submaximal activation. Thus, submaximal parameters of muscle function provide relevant physiological information. To test whether submaximal force generation is affected in muscle from *TPM3*-based myopathy patients, we measured active force at a range of Ca^{2+} levels and expressed force relative to the maximal force. These experiments were also prompted by previous studies indicating that Tm plays an important role

in regulating Ca^{2+} sensitivity of force generation (1,22,23). Figure 6A depicts an example of active force development of a *TPM3*-based myopathy muscle fiber preparation in response to incremental Ca^{2+}. Interestingly, the obtained force–pCa relations were shifted to the left in muscle fibers from all *TPM3*-based myopathy patients (Fig. 6B, left panel), resulting in significantly increased pCa_{50} values (Fig. 6C). Figure 6B (right panel) illustrates that the leftward shift of the relative force versus pCa relations in patients results in absolute force generation at submaximal Ca^{2+} concentrations that is quite comparable between patient and control muscle fiber preparations. [Note that fibers from T7 had too much force rundown (>10%), which might indicate minor structural damage that was not visible on confocal and ultrastructural examination and were therefore excluded from analysis.] Thus, muscle fibers from *TPM3*-based myopathy patients display significantly elevated Ca^{2+} sensitivity of force generation. Interestingly, this contrasts with previous work on patients with nebulin gene mutations, who displayed markedly reduced Ca^{2+} sensitivity of force generation (11).

DISCUSSION

Our findings demonstrate that patients with *TPM3*-based myopathy display a contractile phenotype that is distinct from that of patients with *NEB*-based myopathy. Whereas both show severe myofilament-based muscle weakness, the contractile dysfunction in *TPM3*-based myopathy can be largely explained by changes in cross-bridge cycling kinetics, whereas dysregulation of thin filament length and altered cross-bridge cycling kinetics play a prominent role in *NEB*-based myopathy (6). Furthermore, the loss of force-generating capacity in *TPM3*-based myopathy appears to be partly compensated by enhanced thin filament activation, whereas decreased thin filament activation further depresses the capacity for force production in *NEB*-based myopathy (11).

No major changes in Tm protein in *TPM3*-based myopathy

Tm are actin-binding, coiled-coil proteins, and their major function in skeletal muscle is to stabilize actin and to regulate actin–myosin interactions by limiting access to myosin-binding sites along the major groove of the actin filament (1). In humans, Tms are encoded by four genes, *TPM1–4*, which also undergo extensive alternative splicing (24). The three major Tm gene products expressed in skeletal muscle are α-Tm_{fast} (*TPM1*), β-Tm (*TPM2*) and α-Tm_{slow} (*TPM3*). As the name implies, the *TPM3* gene encodes an isoform that is primarily expressed in type 1 skeletal fibers, but that is also found in type 2A fibers (25). Our analysis of Tm expression and muscle fiber function in five patients with *TPM3*-based myopathy included three who were diagnosed with CFTD and two with NM. Clinically, these two groups are indistinguishable, and the only pathological distinction is whether or not nemaline rods were present in the muscle biopsy that was obtained. In fact, in some families segregating a single *TPM3* mutation, there have been multiple affected members with each of these two diagnoses, suggesting that the underlying pathogenetic mechanisms of these conditions are similar (17). In all five muscle biopsies examined, the mutations in *TPM3* did not affect the ratios of α-Tm expression relative to β-Tm, or total Tm expression relative to actin, the major constituent of the sarcomeric thin filament (Fig. 1). Interestingly, this contrasts with a previous report (26) that the levels of β-Tm were specifically reduced in murine and patient muscles harboring the *TPM3* M9R mutation, a variant not examined in the present study. Regardless, these findings suggest that mutant α-Tm_{slow} is not degraded but is incorporated into the thin filament where it likely exerts its pathogenic influence in a dominant-negative fashion. Two of the five patients, both described previously (16,19), harbor a mutation of the normal stop codon leading to production of an abnormally large protein (Fig. 1A, arrows). Interestingly, whereas one of these patients was diagnosed with CFTD, the other carried a diagnosis of NM. Together with the structural and functional data on the biopsies from these two patients, as well as those on the other three CFTD and NM patients, these findings suggest that patients with *TPM3*-based CFTD do not display a proteomic or functional phenotype that is significantly distinct from that of patients with *TPM3*-based NM. Moreover, as also reported previously (17,19,21), the distinctive feature of CFTD, i.e. selective type 1 fiber hypotrophy (type I fibers >47% smaller than type 2 fibers), was indeed observed in both the three *TPM3*-based CFTD patients studied here and also in the *TPM3*-based NM patients (Fig. 4). As the main distinction between the CFTD and the NM patients is the presence of nemaline rods within the muscle fibers of NM patients, we speculate that these rods might be not much more than a reflection of disease progression or variability in local pathophysiology from one muscle to the next. Longitudinal studies on patients with *TPM3*-based myopathy are needed to test the validity of this speculation.

Dramatic changes in myofilament function in *TPM3*-based myopathy

In the present study, we evaluated skeletal muscle function in demembranated (or skinned) muscle fiber preparations. Because of the young age of some patients at time of biopsy (16,19) and the selective hypotrophy of type 1 fibers, most type 1 fibers were extremely small, precluding experiments on single muscle fibers. Instead, we used myofiber preparations containing bundles of 10–20 muscle fibers. In skinned myofibers, the membranous structures, such as the sarcolemma and sarcoplasmic reticulum, are made permeable, while leaving the myofilaments intact. By exposing these skinned fibers to exogenous Ca^{2+}, their contractile performance was evaluated. These experiments revealed a dramatic (>50%) reduction in the force-generating capacity of myofilaments from patients with *TPM3*-based myopathy, even when force was normalized to fiber CSA (Fig. 2). These data demonstrate that the cause of muscle weakness is primarily myofilament-based, and not secondary to loss of contractile apparatus, defects in excitation–contraction coupling or defects in other aspects of muscle contraction. Furthermore, the weakness in *TPM3*-based myopathy is not caused by major changes in myofibrillar structure, fractional cross-sectional myofibrillar area, or in thin filament length, as evidenced by electron microscopic and functional examination of patients' muscle fibers (Figs 3 and 4). de Haan *et al*. (27)

Table 1. Muscle biopsies and clinical and molecular findings in patients with TPM3 mutations

Patient ID	Biopsy ID	Biopsy location/ age at biopsy	TPM3 mutation	Protein change	Diagnosis	Inheritance	Sex	Presentation
13-2	T7	Quadriceps/5 y/o	c.[855-1G > A] + [857A > C]	p.[=] + p.[X286SerextX*57]	NM	AR	M	Hypotonic at birth, wheelchair by 6 y/o
311-1	T239	Quadriceps/6 m/o	c.[=] + [721G > A]	p.Glu241Lys	CFTD	*De novo* AD	F	Motor delay by 4 m/o, weak and cannot run at 9 y/o
313-1	T261	Quadriceps/1 y/o	c.[857A > C] + [857A > C]	p.X286SerextX*57	CFTD	AR	F	Motor delay and hypotonia by 3 m/o, never walked and ventilator-dependent at 9 y/o
343-1	T856	Biceps/60 y/o	c.[=] + [503G > A]	p.Arg168His	NM	AD	M	Diagnosed after respiratory failure at 58 y/o; mild weakness at time of death (at 66 y/o) of unrelated disease
913-1	T863	Quadriceps/6 m/o	c.[=] + [272G > C]	p.Arg91Pro	CFTD	*De novo* AD	F	Motor delay and hypotonia by 2 m/o, diffusely weak and non-ambulatory at 14 m/o

Nucleotide numbering reflects cDNA number with +1 corresponding to the A of the ATG translation codon. GenBank accession NM_152263.2. NM, nemaline myopathy; CFTD, congenital fiber-type disproportion; y/o, years old; m/o, months old. Note, the splicing mutation, c.855-1G > A, in patient 13-2 was shown to cause loss of the normally spliced product, with low levels of an alternatively spliced, normally sized protein, but the pathogenic mechanism of this recessive change is likely to result from the relative absence of this product. Information in this table has been reported previously (16,19).

have reported reduced isometric force production from intact muscles of *Tpm3* M9R transgenic mice at lower lengths; however, the identical force–SL relationship observed in the present study demonstrates that this is not related to perturbations in thin or think filament lengths. Of note, since our contractile experiments were performed on preparations containing 10–20 muscle fibers and considering that type 1 fibers were hypotrophic (Fig. 4, Table 1), the majority of the preparations (~75%) were comprised of type 2A fibers. Although type 2A fibers mainly express α-Tm_{fast} and β-Tm, they also coexpress α-Tm_{slow} (*TPM3*) (25). Thus, although we cannot rule out the possibility of secondary compensatory or pathological changes in some fast fibers, we propose that the contractile deficit in type 1 and 2A fibers from patients with *TPM3*-based myopathy largely represents a primary effect of the mutated Tm.

To determine the molecular basis for the myofilament-based loss of force-generating capacity in *TPM3*-based myopathy, we examined cross-bridge cycling kinetics. During this cycle, unbound non-force-generating cross-bridges move to an actin-bound force-generating state followed by ATP-driven cross-bridge release back to the non-force-generating state (28,29). Thus, the force that a muscle can generate is proportional to the force generated per cross-bridge as well as to the fraction of cross-bridges that generate force. Whether the fraction of force-generating cross-bridges is different between muscle fibers from patients and control subjects can be evaluated from k_{tr} and tension cost measurements. For such evaluation, we used the analytical framework proposed by Brenner and Eisenberg (30). In this model, the tension cost (ATP consumption rate normalized to tension and fiber volume) is directly proportional to the detachment rate (g_{app}) of myosin cross-bridges from actin. Thus, the increased tension cost in patient fibers (Fig. 5B) indicates that the detachment rate is increased in these fibers. In this framework, the rate constant of force redevelopment (k_{tr}) is proportional to the attachment rate $f_{app} + g_{app}$, and the fraction of cross-bridges attached to actin, to $f_{app}/(f_{app} + g_{app})$. The decrease in k_{tr} of fibers from patients with *TPM3*-based myopathy, together with the notion that g_{app} is increased, indicates that f_{app} must be reduced and that the reduction must be larger than the increase in g_{app}. Overall, this implies that the fraction of force-generating cross-bridges is reduced in patient fibers, contributing to the force deficit observed in these muscle.

A surprising finding was the enhanced thin filament activation, as indicated by the elevated Ca^{2+} sensitivity of force generation, in patients with *TPM3*-based myopathy. As shown in Figure 6B (left panel), muscle fibers from patients generated much higher relative force than control subjects at the same submaximal Ca^{2+} concentration. In contrast to our present findings, previous work on *TPM1* modeling the *TPM3* NM mutation M9R (22,23), and on NM patients with a *TPM2* mutation (encoding β-Tm) (31), reported a decrease in the Ca^{2+} sensitivity of force generation. This discrepancy between studies might lie in differing effects of the specific mutations on Tm function, or on the different isoforms and experimental systems employed, as the other studies either utilized cell-free or cell-based systems with heterologous expression of cardiac isoforms or, in the case of the *TPM2* mutation, caused a change in the relative expression of

β-Tm and α-Tm, whereas such an effect was not observed in the patients studied here which carried a *TPM3* mutation. Interestingly, cardiac papillary myofiber bundles from transgenic mice expressing a familial hypertrophic cardiomyopathy-causing mutation of *Tpm1*, D175N, exhibited enhanced Ca^{2+} sensitivity of force generation similar to that observed in our *TPM3*-mutated skeletal muscle myofiber bundles, illustrating that different Tm mutations appear to affect contraction through different mechanisms (32).

The augmented response to submaximal Ca^{2+} concentrations in the patients with *TPM3*-based myopathy might compensate for the loss of the myofilaments' maximal force-generating capacity. Such a compensatory effect can be illustrated by plotting absolute force (not relative force) against pCa as shown in Figure 6B (right panel). During maximal tetanic muscle activation *in vivo*, the free Ca^{2+} concentration in the muscle fiber rises from a resting level of 10^{-7} M (pCa 7) to 10^{-5} M (pCa 5) at the height of a maximal contraction. However, during normal daily-life, skeletal muscle typically performs submaximal contractions during which the intracellular calcium Ca^{2+} concentration most likely rises to only $1-5 \times 10^{-6}$ M (33). Due to the pronounced leftward shift of the force–pCa relationship at these Ca^{2+} concentrations, the loss of force-generating capacity of muscle fibers from patients with *TPM3*-based myopathy is blunted. Also note that at these submaximal Ca^{2+} concentrations patient T856 generates force that is very close to the force generated by controls (Fig. 6B, right panel). Thus, in this patient, the compensatory effect of increased thin filament activation is likely to explain the relatively mild phenotype of the patient. This patient was not diagnosed until the age of 58 years, and the patient remained ambulatory until death from unrelated causes at age 66, unlike the other four patients who were diagnosed at childhood and who were non-ambulatory already at a very young age (Table 1).

Clinical relevance

Although muscle weakness is considered a hallmark feature of *TPM3*-based myopathy, its pathogenesis is poorly understood. The present study is the first to show a genotype–functional phenotype correlation in patients with different *TPM3* mutations. Remarkably, despite the common occurrence of nemaline rods in both conditions, the mechanical basis for weakness caused by *TPM3* mutations is distinctly different from that observed in *NEB*-based myopathy. These findings provide important novel insights into the pathogenesis of the muscle weakness associated with *TPM3*-based myopathy and provide a scientific basis for differential therapeutics aimed at restoring contractile performance in patients with *TPM3*-based versus *NEB*-based myopathy. For instance, patients with *NEB*-based myopathy might benefit from Ca^{2+} sensitizers, whereas patients with *TPM3*-based myopathy might benefit from pharmaceutical agents that accelerate cross-bridge cycling kinetics.

MATERIALS AND METHODS

Muscle biopsies from patients with *TPM3*-based myopathy

Skeletal muscle specimens, remaining from diagnostic procedures or obtained during clinically indicated surgical procedures, were collected from five patients following informed consent supervised by the Children's Hospital Boston institutional review board and from four unaffected control subjects (three males), with ages that range from 31 to 44 years, all quadriceps biopsies, and stored frozen and unfixed at −80°C until use. For patient characteristics, see Table 1. All five patients had mutations in the *TPM3* gene, have been described previously by either Wattanasirichaigoon *et al*. (Patient 13-2/biopsy T7) (16) or Lawlor *et al*. (Patient 311-1/biopsy T239; Patient 313-1/biopsy T261; Patient 343-1/biopsy T856; Patient 913-1/biopsy T863) (19) and have been entered in the Leiden Open Variation Database (LOVD) available at http://www.dmd.nl/nmdb2/home.php?select_db=TPM3 (see Table 1 for a synopsis of clinical findings).

Protein analyses

For Tm expression, western blotting was performed using an antibody directed against both α- and β-Tm (CH1, Hybridoma Bank, University of Iowa). Secondary antibodies conjugated with fluorescent dyes with infrared excitation spectra were used for detection. One- or two-color infrared western blots were scanned (Odyssey Infrared Imaging System, Li-Cor Biosciences, NE, USA) and the images analyzed with One-D scan EX. For myosin heavy chain isoform composition, skeletal muscles were denatured by boiling for 2 min. The stacking gel contained a 4% acrylamide concentration (pH 6.7), and the separating gel contained 7% acrylamide (pH 8.7) with 30% glycerol (v/v). The gels were run for 24 h at 15°C and a constant voltage of 275 V. Finally, the gels were silver-stained, scanned and analyzed with One-D scan EX software.

Muscle mechanics

Small strips dissected from muscle biopsies were skinned overnight. The skinning procedure renders the membranous structures in the muscle fibers permeable, which enables activation of the myofilaments with exogenous Ca^{2+}. Preparations were washed thoroughly with relaxing solution and stored in 50% glycerol/relaxing solution at −20°C for up to ∼8 weeks. Muscle fibers or small muscle bundles (diameter ∼0.07 mm) were dissected from the skinned strips and were mounted between a displacement generator and a force transducer element (AE 801, SensoNor, Norway) using aluminum T-clips. For all contractile parameters, 6–10 preparations were analyzed per subject. SL was set using a HeNe laser-diffraction system. Mechanical experiments on contracting muscle were carried out at an SL of ∼2.5 μm. Fiber width and diameter were measured at three points along the fiber, and the CSA was determined assuming an elliptical cross-section. Three different bathing solutions were used during the experimental protocols: a relaxing solution, a pre-activating solution with low ethyleneglycotetraacetic acid (EGTA) concentration, and an activating solution (pCa 4.5). The composition of these solutions was as described previously (34). The preparation was activated at pCa 4.5 to obtain maximal Ca^{2+}-activated force. Maximal stress was determined by dividing the force generated at pCa 4.5 by CSA. To determine force–SL relations, the maximal force

generated at various SLs was determined. SL was measured with an online laser-diffraction system (35).

Force–pCa relations. To determine the force–pCa relation (pCa = −log of molar free Ca^{2+} concentration), skinned muscle fiber bundles were sequentially bathed in solutions with pCa values ranging from 4.5 to 9.0 and the steady-state force was measured. Measured force values were normalized to the maximal force obtained at pCa 4.5. The obtained force–pCa data were fit to the Hill equation, providing pCa_{50} (pCa giving 50% maximal active tension) and the Hill coefficient, n_H, an index of myofilament cooperativity.

k_{tr} measurements. To measure the rate of tension redevelopment (k_{tr}) in muscle fiber bundles, we used the large slack/release approach (30) to disengage force-generating cross-bridges from the thin filaments, which were isometrically activated. Fast activation of the fiber was achieved by transferring the skinned muscle fibers from the pre-activation solution containing a low concentration of EGTA (pCa 9.0) to a pCa 4.5 activating solution. Once the steady-state was reached, a slack equivalent to 20% of the muscle length was rapidly induced at one end of the muscle using the motor. This was followed immediately by an unloaded shortening lasting 30 ms. The remaining bound cross-bridges were mechanically detached by rapidly (1 ms) restretching the muscle fiber to its original length, after which tension redevelops. The rate constant of monoexponential tension redevelopment (k_{tr}) was determined by fitting the rise of tension to the following equation: $F = F_{ss}(1 - e^{-k_{tr}t})$, where F is the force at time t, F_{ss} the steady-state force and k_{tr} the rate constant of tension redevelopment. (Note that fibers from T856 broke during these measurements, and, therefore, we could not determine the k_{tr} values for this patient. Although microscopic examination indicated normal myofibrillar structure, we cannot rule out that the minor structural damage in T856 increased the fibers' sensitivity to mechanical perturbations.)

Simultaneous force–ATPase measurement. We used the system described by Stienen *et al*. (34). To measure the ATPase activity, a near UV light was projected through the window of the bath (30 μl volume and temperature controlled at 20°C) and detected at 340 nm. The maximum activation buffer (pCa 4.5) contained 10 mM phosphoenol pyruvate, with 4 mg ml^{-1} pyruvate kinase (500 U mg^{-1}), 0.24 mg ml^{-1} lactate dehydrogenase (870 U mg^{-1}) and 20 μM diadenosine-5′ pentaphosphate (A_2P_5). For efficient mixing, the solution in the bath was continuously stirred by means of motor-driven vibration of a membrane positioned at the base of the bath. ATPase activity of the skinned fiber bundles was measured as follows: ATP regeneration from adenosine diphosphate (ADP) is coupled to the breakdown of phosphoenol pyruvate to pyruvate and ATP catalyzed by pyruvate kinase, which is linked to the synthesis of lactate catalyzed by lactate dehydrogenase. The breakdown of NADH, which is proportional to the amount of ATP consumed, is measured on-line by UV absorbance at 340 nm. The ratio of light intensity at 340 nm (sensitive to NADH concentration), and the light intensity at 400 nm (reference signal), is obtained by means of an analog divider. After each recording, the UV absorbance signal of NADH was calibrated by multiple rapid injections of 0.25 nmol of ADP (0.025 μl of 10 mM ADP) into the bathing solution, with a stepper motor-controlled injector. The slope of the [ATP] versus time trace during steady-state tension development of a Ca^{2+}-induced contraction (Fig. 5A) was determined from a linear fit and the value divided by the fiber volume (in mm^3) to determine the fiber's ATPase rate. ATPase rates were corrected for the basal ATPase measured in relaxing solution. The ATPase rate was divided by tension (force/CSA) to determine the tension cost.

Immunofluorescence confocal scanning laser microscopy

Small strips were dissected from the biopsies and skinned overnight at ∼4°C in relaxing solution (in mM; 20 N,N-bis (2 -hydroxy-ethyl)-2-aminoethanesulfonic acid, 10 EGTA, 6.56 $MgCl_2$, 5.88 NaATP, 1 dithiothreitol, 46.35 K-propionate, 15 creatine phosphate, pH 7.0 at 20°C) containing 1% (v/v) Triton X-100. Immunolabeling and confocal scanning laser microscopy was performed essentially as described previously (3). Primary antibodies: anti-α-actinin (mouse monoclonal, A7811, Sigma-Aldrich), anti-tropomodulin-1 (3) and Alexa Fluor 488 conjugated phalloidin (A12379, Invitrogen). Secondary antibodies: Alexa Fluor 594 (goat anti-mouse, Invitrogen) and Alexa Fluor 488 (goat anti-rabbit, Invitrogen). Secondary antibodies did not stain when used without primary antibodies (data not shown). Images were produced using a Bio-Rad MRC 1024 confocal laser scanning microscope using the LaserSHARP 2000 software package (Hercules, CA, USA). From the acquired images, thin filament lengths were determined using ImageJ software (National Institutes of Health). Approximately three preparations were analyzed per subject.

Pathological evaluation

Muscle biopsy tissue was obtained and prepared using the standard histological protocols (36). Briefly, fresh muscle was frozen in isopentane, cooled in liquid nitrogen and stored at −80°C until sectioning. Eight micrometer histological sections were cut on a cryostat, and sections were stained with either hematoxylin and eosin, Gomori trichrome, ATPase (at pH 4.3 and 9.2) or NADH. Histological findings in these patients using these stains have been reported previously (16,19). A small portion of tissue from four patients (T7, T261, T856 and T863) was fixed, embedded in Epon and processed for electron microscopy per standard histological techniques. Epon-embedded tissue was sectioned at 1 μm thickness and stained with toluidine blue. Photomicrographs of toluidine blue-stained sections were obtained using a Nikon Eclipse 50i microscope with SPOT Insight 4 Meg FW Color Mosaic camera and SPOT 4.5.9.1 software from Diagnostic Instruments. Ultrastructural examination was performed on lead-stained, 95 nm sections at the time of biopsy and repeated on three patients (T261, T856 and T863) for preparation of this manuscript. Photographs and a report of the electron microscopy of tissue from patient T7 were reviewed, but tissue was not available for additional ultrastructural studies.

Statistical analysis

The data are presented as the mean ± SEM. Statistical analyses were performed by *t*-test, and where appropriate by

one-way ANOVA followed by Bonferroni *post hoc* testing; $P < 0.05$ was considered as statistically significant.

Conflict of Interest statement. None declared.

FUNDING

This work was funded by a VENI grant from the Dutch Organization for Scientific Research, as well as National Institutes of Health grants R01 AR044345, RO1 AR053897, K08 AR059750 and L40 AR057721 from the NIAMS and P50 NS040828 from the NINDS, and by generous support from the Joshua Frase Foundation, and the Lee and Penny Anderson Family Foundation.

REFERENCES

1. Gordon, A.M., Homsher, E. and Regnier, M. (2000) Regulation of contraction in striated muscle. *Physiol. Rev.*, **80**, 853–924.
2. Granzier, H.L., Akster, H.A. and Ter Keurs, H.E. (1991) Effect of thin filament length on the force-sarcomere length relation of skeletal muscle. *Am. J. Physiol.*, **260**, C1060–C1070.
3. Witt, C.C., Burkart, C., Labeit, D., McNabb, M., Wu, Y., Granzier, H. and Labeit, S. (2006) Nebulin regulates thin filament length, contractility, and Z-disk structure in vivo. *EMBO J.*, **25**, 3843–3855.
4. Ottenheijm, C.A. and Granzier, H. (2010) Lifting the nebula: novel insights into skeletal muscle contractility. *Physiology*, **25**, 304–310.
5. Bang, M.L., Li, X., Littlefield, R., Bremner, S., Thor, A., Knowlton, K.U., Lieber, R.L. and Chen, J. (2006) Nebulin-deficient mice exhibit shorter thin filament lengths and reduced contractile function in skeletal muscle. *J. Cell Biol.*, **173**, 905–916.
6. Ottenheijm, C.A., Witt, C.C., Stienen, G.J., Labeit, S., Beggs, A.H. and Granzier, H. (2009) Thin filament length dysregulation contributes to muscle weakness in nemaline myopathy patients with nebulin deficiency. *Hum. Mol. Genet.*, **18**, 2359–2369.
7. Laing, N.G. and Nowak, K.J. (2005) When contractile proteins go bad: the sarcomere and skeletal muscle disease. *Bioessays*, **27**, 809–822.
8. Agrawal, P.B., Greenleaf, R.S., Tomczak, K.K., Lehtokari, V.L., Wallgren-Pettersson, C., Wallefeld, W., Laing, N.G., Darras, B.T., Maciver, S.K., Dormitzer, P.R. and Beggs, A.H. (2007) Nemaline myopathy with minicores caused by mutation of the CFL2 gene encoding the skeletal muscle actin-binding protein, cofilin-2. *Am. J. Hum. Genet.*, **80**, 162–167.
9. Sanoudou, D. and Beggs, A.H. (2001) Clinical and genetic heterogeneity in nemaline myopathy—a disease of skeletal muscle thin filaments. *Trends Mol. Med.*, **7**, 362–368.
10. Pelin, K., Hilpela, P., Donner, K., Sewry, C., Akkari, P.A., Wilton, S.D., Wattanasirichaigoon, D., Bang, M.L., Centner, T., Hanefeld, F. *et al.* (1999) Mutations in the nebulin gene associated with autosomal recessive nemaline myopathy. *Proc. Natl Acad. Sci. USA*, **96**, 2305–2310.
11. Ottenheijm, C.A., Hooijman, P., Dechene, E.T., Stienen, G.J., Beggs, A.H. and Granzier, H. (2010) Altered myofilament function depresses force generation in patients with nebulin-based nemaline myopathy (NEM2). *J. Struct. Biol.*, **170**, 334–343.
12. Chandra, M., Mamidi, R., Ford, S., Hidalgo, C., Witt, C., Ottenheijm, C., Labeit, S. and Granzier, H.L. (2009) Nebulin alters crossbridge cycling kinetics and increases thin filament activation—a novel mechanism for increasing tension and reducing tension cost. *J. Biol. Chem.*, **284**, 30889–30896.
13. Bang, M.L., Caremani, M., Brunello, E., Littlefield, R., Lieber, R.L., Chen, J., Lombardi, V. and Linari, M. (2009) Nebulin plays a direct role in promoting strong actin-myosin interactions. *FASEB J.*, **23**, 4117–4125.
14. Laing, N.G., Majda, B.T., Akkari, P.A., Layton, M.G., Mulley, J.C., Phillips, H., Haan, E.A., White, S.J., Beggs, A.H., Kunkel, L.M. *et al.* (1992) Assignment of a gene (NEMI) for autosomal dominant nemaline myopathy to chromosome I. *Am. J. Hum. Genet.*, **50**, 576–583.
15. Laing, N.G., Wilton, S.D., Akkari, P.A., Dorosz, S., Boundy, K., Kneebone, C., Blumbergs, P., White, S., Watkins, H., Love, D.R. *et al.* (1995) A mutation in the alpha tropomyosin gene TPM3 associated with autosomal dominant nemaline myopathy. *Nat. Genet.*, **9**, 75–79.
16. Wattanasirichaigoon, D., Swoboda, K.J., Takada, F., Tong, H.Q., Lip, V., Iannaccone, S.T., Wallgren-Pettersson, C., Laing, N.G. and Beggs, A.H. (2002) Mutations of the slow muscle alpha-tropomyosin gene, TPM3, are a rare cause of nemaline myopathy. *Neurology*, **59**, 613–617.
17. Clarke, N.F., Kolski, H., Dye, D.E., Lim, E., Smith, R.L., Patel, R., Fahey, M.C., Bellance, R., Romero, N.B., Johnson, E.S. *et al.* (2008) Mutations in TPM3 are a common cause of congenital fiber type disproportion. *Ann. Neurol.*, **63**, 329–337.
18. Lehtokari, V.L., Pelin, K., Donner, K., Voit, T., Rudnik-Schoneborn, S., Stoetter, M., Talim, B., Topaloglu, H., Laing, N.G. and Wallgren-Pettersson, C. (2008) Identification of a founder mutation in TPM3 in nemaline myopathy patients of Turkish origin. *Eur. J. Hum. Genet.*, **16**, 1055–1061.
19. Lawlor, M.W., Dechene, E.T., Roumm, E., Geggel, A.S., Moghadaszadeh, B. and Beggs, A.H. (2010) Mutations of tropomyosin 3 (TPM3) are common and associated with type 1 myofiber hypotrophy in congenital fiber type disproportion. *Hum. Mutat.*, **31**, 176–183.
20. Rajasekaran, M.R., Jiang, Y., Bhargava, V., Littlefield, R., Lee, A., Lieber, R.L. and Mittal, R.K. (2008) Length-tension relationship of the external anal sphincter muscle: implications for the anal canal function. *Am. J. Physiol. Gastrointest. Liver Physiol.*, **295**, G367–G373.
21. Ryan, M.M., Ilkovski, B., Strickland, C.D., Schnell, C., Sanoudou, D., Midgett, C., Houston, R., Muirhead, D., Dennett, X., Shield, L.K. *et al.* (2003) Clinical course correlates poorly with muscle pathology in nemaline myopathy. *Neurology*, **60**, 665–673.
22. Michele, D.E., Albayya, F.P. and Metzger, J.M. (1999) A nemaline myopathy mutation in alpha-tropomyosin causes defective regulation of striated muscle force production. *J. Clin. Invest.*, **104**, 1575–1581.
23. Moraczewska, J., Greenfield, N.J., Liu, Y. and Hitchcock-DeGregori, S.E. (2000) Alteration of tropomyosin function and folding by a nemaline myopathy-causing mutation. *Biophys. J.*, **79**, 3217–3225.
24. Lees-Miller, J.P. and Helfman, D.M. (1991) The molecular basis for tropomyosin isoform diversity. *Bioessays*, **13**, 429–437.
25. Oe, M., Nakajima, I., Muroya, S., Shibata, M. and Chikuni, K. (2009) Relationships between tropomyosin and myosin heavy chain isoforms in bovine skeletal muscle. *Anim. Sci. J.*, **80**, 193–197.
26. Corbett, M.A., Akkari, P.A., Domazetovska, A., Cooper, S.T., North, K.N., Laing, N.G., Gunning, P.W. and Hardeman, E.C. (2005) An alpha-tropomyosin mutation alters dimer preference in nemaline myopathy. *Ann. Neurol.*, **57**, 42–49.
27. de Haan, A., van der Vliet, M.R., Gommans, I.M., Hardeman, E.C. and van Engelen, B.G. (2002) Skeletal muscle of mice with a mutation in slow alpha-tropomyosin is weaker at lower lengths. *Neuromuscul. Disord.*, **12**, 952–957.
28. Huxley, A.F. and Simmons, R.M. (1971) Proposed mechanism of force generation in striated muscle. *Nature*, **233**, 533–538.
29. Lymn, R.W. and Taylor, E.W. (1971) Mechanism of adenosine triphosphate hydrolysis by actomyosin. *Biochemistry*, **10**, 4617–4624.
30. Brenner, B. and Eisenberg, E. (1986) Rate of force generation in muscle: correlation with actomyosin ATPase activity in solution. *Proc. Natl Acad. Sci. USA*, **83**, 3542–3546.
31. Ochala, J., Li, M., Ohlsson, M., Oldfors, A. and Larsson, L. (2008) Defective regulation of contractile function in muscle fibres carrying an E41K beta-tropomyosin mutation. *J. Physiol.*, **586**, 2993–3004.
32. Muthuchamy, M., Pieples, K., Rethinasamy, P., Hoit, B., Grupp, I.L., Boivin, G.P., Wolska, B., Evans, C., Solaro, R.J. and Wieczorek, D.F. (1999) Mouse model of a familial hypertrophic cardiomyopathy mutation in alpha-tropomyosin manifests cardiac dysfunction. *Circ. Res.*, **85**, 47–56.
33. Allen, D.G., Lamb, G.D. and Westerblad, H. (2008) Skeletal muscle fatigue: cellular mechanisms. *Physiol. Rev.*, **88**, 287–332.
34. Stienen, G.J., Kiers, J.L., Bottinelli, R. and Reggiani, C. (1996) Myofibrillar ATPase activity in skinned human skeletal muscle fibres: fibre type and temperature dependence. *J. Physiol.*, **493** (Pt 2), 299–307.
35. Granzier, H.L. and Wang, K. (1993) Interplay between passive tension and strong and weak binding cross-bridges in insect indirect flight muscle. A functional dissection by gelsolin-mediated thin filament removal. *J. Gen. Physiol.*, **101**, 235–270.
36. Dubowitz, V. and Sewry, C. (2007) *Muscle Biopsy: A Practical Approach*. Saunders.